

PAPER

[View Article Online](#)
[View Journal](#) | [View Issue](#)Cite this: *RSC Chem. Biol.*, 2024, 5, 914Received 9th May 2024,
Accepted 22nd July 2024

DOI: 10.1039/d4cb00105b

rsc.li/rsc-chembioDiscovery of a new inhibitor for YTH domain-containing m⁶A RNA readers†

Chuan-Hui Wang and Huiqing Zhou *

N⁶-methyladenosine (m⁶A) is an abundant modification in mammalian mRNAs and plays important regulatory roles in gene expression, primarily mediated through specific recognition by “reader” proteins. YTH family proteins are one major family of known m⁶A readers, which specifically recognize m⁶A-modified transcripts via the YTH domains. Despite the significant relevance of YTH-m⁶A recognition in biology and diseases, few small molecule inhibitors are available for specifically perturbing this interaction. Here we report the discovery of a new inhibitor (“N-7”) for YTH-m⁶A RNA recognition, from the screening of a nucleoside analogue library against the YTH domain of the YTHDF1 protein. N-7 is characterized to be a *pan*-inhibitor *in vitro* against five YTH domains from human YTHDF1, YTHDF2, YTHDF3, YTHDC1, and YTHDC2 proteins, with IC₅₀ values in the range of 30–48 μM measured using a fluorescence polarization competition assay. We demonstrated that N-7 directly interacts with the YTH domain proteins via a thermal shift assay. N-7 expands the chemical structure landscape of the m⁶A YTH domain-containing reader inhibitors and potentiates future inhibitor development for reader functional studies and therapeutic efforts in targeting the epitranscriptome.

Introduction

N⁶-methyladenosine (m⁶A) is one of the most abundant internal chemical modifications in eukaryotic messenger RNAs (mRNAs)^{1–4} and it exerts important regulatory functions in mRNA metabolism and gene expression, primarily mediated through direct or indirect recognition by m⁶A “readers”.^{5–13} The m⁶A “readers” refer to RNA binding proteins that bind to m⁶A-modified RNAs with much greater affinity than to unmodified RNAs.^{14,15} The YT521-B homology (YTH) family of proteins, including YTHDF1-3, YTHDC1, and YTHDC2, are the first reported and the most extensively studied m⁶A readers.^{3,7} YTH family proteins contain a YTH domain at or close to the C-termini of the full-length protein, which is responsible for m⁶A RNA recognition (Fig. 1A). *In vitro* binding studies showed that the purified YTH domains from YTHDF1-3 and YTHDC1 bind m⁶A-modified RNA oligonucleotides with micromolar binding affinities that are 10–100 fold tighter than binding with unmodified RNAs that carry the same sequences.^{16,17} High-resolution structures of the recognition complexes between m⁶A RNA and the YTH domains revealed that YTH domains directly recognize m⁶A through a hydrophobic binding pocket that contains two or three tryptophan residues (Fig. 1A); additionally, the YTH

domain also presents a cleft that is rich in basic residues that present electrostatic interactions with the RNA backbone.^{14,17–23}

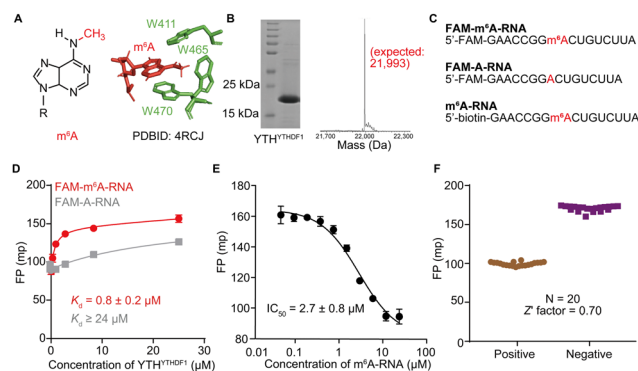


Fig. 1 Screening YTH^{YTHDF1} inhibitors by FP competition assay. (A) The chemical structure of m⁶A (left) and hydrophobic binding pocket of YTH^{YTHDF1} (right). (B) SDS-PAGE and MS characterizations of the purified YTH^{YTHDF1} protein. The gel image of the purified protein with Coomassie Blue staining (left) and the deconvolution mass data (right) and the theoretical expected mass (in red) of the purified protein are shown. (C) Sequences of three RNA oligonucleotides: FAM-m⁶A-RNA, FAM-A-RNA, and m⁶A-RNA were used in the FP assay. (D) The FP binding data and fitted binding curves for YTH^{YTHDF1} and FAM-m⁶A-RNA or FAM-A-RNA. Data are presented as mean ± standard deviation (SD) with *n* = 3 biological replicates. (E) The displacement of FAM-m⁶A-RNA from YTH^{YTHDF1} by the non-fluorescent m⁶A-RNA by the FP competition assay with the fitted IC₅₀ value. Data are presented as mean ± SD with *n* = 3 biological replicates. (F) The data for the determination of Z' factor based on *N* = 20 repeated measurements of the FP competition assay for screening.

Department of Chemistry, Merkert Chemistry Center, Boston College, Chestnut Hill, MA 02467, USA. E-mail: zhouqf@bc.edu

† Electronic supplementary information (ESI) available. See DOI: <https://doi.org/10.1039/d4cb00105b>

Alongside the m⁶A recognition by the YTH domain, the rest of the regions in the YTH family proteins are involved in sophisticated protein–protein interactions in cells and exert diverse functional consequences of m⁶A RNA recognition by readers. For example, Du *et al.* showed that the N-terminal domain of human YTHDF2 protein directly interacts with the scaffolding subunit CNOT1 in the CCR4–NOT deadenylase complex *via* co-immunoprecipitation assays, which promotes the deadenylation-dependent mRNA decay.¹⁸ This interaction accelerates the decay of m⁶A-modified mRNAs. Meanwhile, the N-terminal domain of YTHDF2 was reported to interact with other proteins including the heat-responsive protein 12 (HRSP12) and the upstream frame-shift 1 (UPF1) protein.^{19,20} Both interactions between YTHDF2 and HRSP12 or UPF1 promote the decay of m⁶A-modified mRNAs through internal cleavage or nonsense-mediated RNA decay, respectively.^{19,20} Besides YTHDF2, the functions of YTH family proteins are involved in many biological transactions, including RNA decay,¹⁰ nuclear export,⁸ RNA splicing,²¹ translation,^{10,11} transcription,¹³ and the formation and functions of large ribonucleoprotein complex assemblies such as stress granules and P bodies.^{18,22–24}

In addition to the intricate protein–protein interaction network that YTH proteins are involved in, the YTH domains were reported to recognize substrates beyond m⁶A RNA *in vitro* and *in cellulo*, including m¹A^{25,26} and N⁶-methyldeoxyadenosine (6mA) in DNA.²⁷ All these factors complicate the studies of the precise functional roles of YTH family proteins and chemical modifications in physiology and diseases. Indeed, dysregulated expression levels of YTH proteins frequently occur in embryonic development,¹³ neuronal development,²⁸ memory formation,²⁹ multiple aspects of cancer biology,^{30,31} and viral infections.³² The current experimental strategies to study the biological consequences of YTH family proteins primarily rely on the knockdown, knockout, or overexpression of a YTH protein of interest.^{33,34} Such perturbations will concurrently interrupt all interactions the protein may have, making it inconclusive to reason whether the YTH–m⁶A recognition is causative for the observed biological consequence.

The development of small molecule inhibitors that specifically perturb the YTH–m⁶A recognition will provide invaluable insights to dissect the sophisticated interaction network YTH proteins involve and reveal m⁶A-causative YTH functions. Indeed, a recent report by Zou *et al.* identified a natural product salvianolic acid C (SAC) as a selective inhibitor for m⁶A-RNA and YTH^{YTHDF1} with a 20-fold higher observed inhibitory effect compared to YTH^{YTHDF2} *via* AlphaScreen assays *in vitro*,³⁵ although the molecular mechanism of the observed selectivity remains to be characterized. SAC contributed to elucidating the function of YTHDF1 in the formation of ribonucleoprotein condensations and translation regulation in neurons.³⁵ Aside from SAC, only a handful of other inhibitors have been reported for YTH and m⁶A recognition.^{36–42} It remains in great demand to explore broader chemical space for inhibitor discoveries and to carry out in-depth characterization of inhibitor selectivity against different YTH family proteins.

Here we report the discovery of an inhibitor for m⁶A–YTH recognition, resulting from the screening of a commercially

available nucleoside analogue library against the YTH domain of YTHDF1 protein. Very interestingly, our screening data identified lead compound structures resembling adenosine, with modifications on the ribose moiety and the N6 position. We chose to further characterize a representative compound N-7, which showed a *pan*-inhibitory effect of m⁶A RNA–YTH recognition for five YTH domains of YTHDF1, YTHDF2, YTHDF3, YTHDC1, and YTHDC2 proteins with IC₅₀ values ranging from 30 to 48 μM. We demonstrated that the inhibitory activity results from the direct interaction between N-7 and the YTH domain proteins *via* thermal shift assay. We systematically compared the inhibitory activity and selectivity against different YTH domains of N-7 to four reported YTH domain inhibitors (SAC,³⁵ m⁶A nucleoside,^{36,37} compound 6,³⁶ and compound 26³⁸). The comparison revealed that N-7 showed competitive inhibitory activity among the reported inhibitors and presented unique *pan*-inhibitory activity against the five YTH domains.

Results and discussion

Screening of inhibitors for YTH^{YTHDF1}–m⁶A RNA recognition

Firstly, we confirmed that the prepared YTH domain of YTHDF1 (denoted as YTH^{YTHDF1}) was an m⁶A reader by measuring the binding affinities of the protein with the synthetic oligonucleotides *via* the fluorescence polarization (FP) binding assay. We over-expressed and purified YTH^{YTHDF1} protein with an N-terminal His tag from *E. coli* cells, and validated the size of the purified protein *via* SDS-PAGE and mass spectrometry (MS) (Fig. 1B and Fig. S1, ESI†). The purified YTH^{YTHDF1} showed binding to the 16-nucleotide (nt) FAM-labeled m⁶A-containing oligonucleotide (“FAM–m⁶A–RNA”) with $K_d = 0.8 \pm 0.2$ μM measured using the FP binding assay (Fig. 1C and D), consistent with the previously reported affinity ($K_d = 1.0 \pm 0.3$ μM) measured using isothermal titration calorimetry (ITC).¹⁴ Meanwhile, we observed significantly weakened binding ($K_d \geq 24$ μM) between the YTH^{YTHDF1} and unmodified RNA with the same sequence (“FAM–A–RNA”) by the FP assay (Fig. 1C and D). During the titration of the purified YTH^{YTHDF1} up to 24 μM in the FP binding assay, the total fluorescence intensities (*i.e.* the sum of the parallel and perpendicular fluorescence intensities) produced by the FAM-labeled RNA oligonucleotides remain stable (Fig. S2A, ESI†), suggesting the FP assay is a suitable assay to quantify the binding between the used RNA oligonucleotides and the YTH domain.

To identify small molecule inhibitors of YTH-domain proteins, we set up an FP competition assay with the purified YTH^{YTHDF1} for the screening. Briefly, 25 nM of FAM–m⁶A–RNA was pre-incubated with 2 μM (greater than 2 times the measured K_d) YTH^{YTHDF1}; an increasing concentration of a non-fluorescent “m⁶A–RNA” (Fig. 1C) was titrated into the pre-formed FAM–m⁶A–RNA:YTH^{YTHDF1} complex, to compete for binding. When the FAM–m⁶A–RNA was competed off the RNA–protein complex, it became free RNA with reduced FP. As expected, we observed decreased FP upon increasing concentrations of the non-fluorescent m⁶A–RNA, with an



$IC_{50} = 2.7 \pm 0.8 \mu M$ (Fig. 1E). Next, we used the non-fluorescent m^6A -RNA and blank binding buffer as the “positive control” and “negative control” competitors to perform the FP competition assay for 20 repeats and the repeated assays generated a Z' factor = 0.7,⁴³ demonstrating the excellent performance of the FP competition assay for screening (Fig. 1F). Additionally, we confirmed that the FP signal was not affected by the addition of 5% DMSO as small molecule libraries were dissolved in 100% DMSO (Fig. S2B, ESI†).

We conducted screening of 320 compounds from a commercially available nucleoside analogue library with the FP competition assay; excitingly, we identified several compounds showing reduced FP relative to the DMSO control when added to the pre-formed FAM- m^6A -RNA:YTH^{YTHDF1} complex at the final compound concentration of 40 μM during the screening, suggesting them as potential binding inhibitors (Fig. 2). Next, we followed up with the top 13 compounds that showed at least a 35% reduction of the FP signal relative to the DMSO control (Fig. 2). Interestingly, the chemical structures of all 13 compounds showed as analogues of adenosine with chemical modifications at the N9 and the N6 of adenine (Fig. S3A, ESI†). Moreover, 7 out of the 13 compounds (N-7, H-14, D-20, D-15, B-16, H-15, N-12) shared the same bis-hydroxymethyl cyclobutyl group at the N9 position (Fig. S3A, ESI†), which increased our confidence in the relevance of the identified structures. We confirmed the reproducibility of the screening results by running the FP competition assay with higher compound dosages at 200 μM with replicates. The 13 compounds all showed a reduction of the FP signal in a dose-response manner (Fig. S3B, ESI†). We chose the compound “N-7”, one of the compounds that showed the most significant inhibitory effect and did not interfere with the total fluorescence intensity of the assay, for further characterizations (Fig. 3A and Fig. S3B, C, ESI†). Meanwhile, we chose the compound “D-6” in the screened library as a negative control. D-6 shares the same purine and the [1-(hydroxymethyl)cyclobutyl]methanol structures with N-7 but contains a 3-propan-2-yl-2-azaspiro[3.5]nonane group, rather than the 2,7-diazaspiro[4.4]nonan-8-one group in N-7 (Fig. 3A). We performed dose-response curve measurements to quantify the inhibitory activity (*i.e.* IC_{50}) of N-7 via the FP

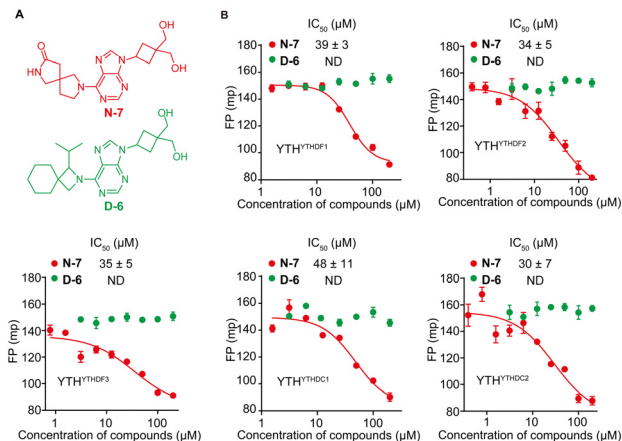


Fig. 3 N-7 is a *pan*-YTH domain inhibitor. (A) The chemical structures of N-7 and D-6. (B) Dose-response curves for the inhibitory activities of N-7 and D-6 against YTH^{YTHDF1}, YTH^{YTHDF2}, YTH^{YTHDF3}, YTH^{YTHDC1}, and YTH^{YTHDC2} proteins, measured using the FP competition assay. Data are presented as mean \pm SD ($n = 3$ replicates). “ND” denotes “not detected by FP competition assay”.

competition assay. N-7 (Fig. S4, ESI†) shows an inhibitory effect on the YTH^{YTHDF1} and FAM- m^6A -RNA binding with an IC_{50} value of $39 \pm 3 \mu M$, whereas D-6 shows no detectable competition (Fig. 3B).

N-7 is a *pan*-YTH-domain inhibitor

Next, we proceeded to examine the selectivity of N-7 against different YTH domains. We over-expressed and purified the YTH domains of human YTHDF2 (YTH^{YTHDF2}), YTHDF3 (YTH^{YTHDF3}), YTHDC1 (YTH^{YTHDC1}), and YTHDC2 (YTH^{YTHDC2}) proteins (Fig. S5–S8, ESI†). First, we confirmed the purified YTH^{YTHDF2}, YTH^{YTHDF3}, YTH^{YTHDC1}, and YTH^{YTHDC2} as m^6A readers *in vitro* by the FP binding assay. The measured binding affinities for all the YTH domains against the m^6A -modified RNA agree with the reported values,^{7,14,17,44} and were significantly higher relative to the binding with the unmodified RNA (Fig. S9A, ESI†). We further benchmarked the FP competition assay for all purified YTH domain proteins with the non-fluorescent m^6A -RNA as the positive control competitor. The results demonstrated that the non-fluorescent m^6A -RNA competes effectively with the FAM- m^6A -RNA in complex with each of the YTH proteins (Fig. S9B, ESI†). We proceeded to test the inhibitory activity for N-7 against m^6A -RNA bound with different YTH domains. Interestingly, N-7 exhibited comparable inhibitory activities against all purified YTH domains, with $IC_{50} = 39 \pm 3 \mu M$ for YTH^{YTHDF1}, $34 \pm 5 \mu M$ for YTH^{YTHDF2}, $35 \pm 5 \mu M$ for YTH^{YTHDF3}, $48 \pm 11 \mu M$ for YTH^{YTHDC1}, and $30 \pm 7 \mu M$ for YTH^{YTHDC2} measured by the FP competition assay (Fig. 3B). The IC_{50} values for N-7 against multiple YTH domains were robustly measured when altering the protein concentration or the order of reagents addition applied in the FP competition assay (Fig. S10, ESI†). In contrast, the negative control compound D-6 did not show competition against m^6A RNA binding to all YTH-domain proteins (Fig. 3B). To further validate the measurements by the FP competition assay, we developed the RNA electrophoretic mobility shift assay (REMSA)⁴⁵ to assess

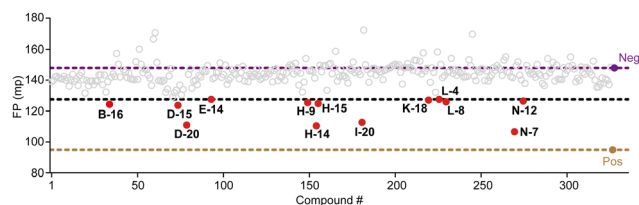


Fig. 2 Screening YTH^{YTHDF1} inhibitors using the FP competition assay. The data of the screening against 320 compounds from the nucleoside mimetics library are shown. The concentration of each compound is 40 μM with two technical replicates. The FP values measured for the positive (“ m^6A -RNA”) and negative controls (“DMSO”) are shown in brown and purple. Compounds are shown in red if they show at least a 35% reduction of FP (cut-off indicated by the black dashed line) relative to the negative control. These compounds are labeled with their IDs in the original library.

inhibitory activity of small molecule inhibitors for YTH-m⁶A RNA binding. We measured the inhibitory activity of N-7 against YTH domains of YTHDF1 and YTHDC1 using REMSA, which yielded an IC₅₀ value of 45 ± 5 μM for YTH^{YTHDF1} and 30 ± 2 μM for YTH^{YTHDC1} (Fig. S11, ESI†). The REMSA results agree with those measured by the FP competition assay within error (Fig. 3B).

Given that N-7 is a *pan*-inhibitor for YTH domains, we investigate its inhibition selectivity against other m⁶A RNA recognition proteins that do not contain a YTH domain. We chose to test FTO, one of the eraser proteins that recognize m⁶A RNA and catalyze the removal of the methylation of m⁶A in the presence of co-factors Fe²⁺ and α-ketoglutarate.⁴⁶ We expressed and purified the FTO protein and confirmed binding between the purified FTO protein and FAM-m⁶A-RNA with the FP assay in the absence of catalytic co-factors (Fig. S12A–D, ESI†). We benchmarked the FP competition assay by measuring the inhibitory activity of a reported FTO inhibitor FB23,⁴⁷ which shows IC₅₀ of 0.6 ± 0.2 μM (Fig. S12E, ESI†). In contrast, N-7 did not show any detectable inhibition against FTO binding with m⁶A-RNA (Fig. S12F, ESI†). This suggests that N-7 shows selective binding to YTH domain proteins over FTO.

Together, these findings show that N-7 is a *pan*-inhibitor for the recognition between YTH domains and m⁶A RNA, and presents selective inhibition against YTH domains over a non-YTH m⁶A recognition protein FTO.

N-7 directly interacts with YTH-domain proteins

To probe the inhibitory mechanism, we assessed interactions between N-7 and FAM-m⁶A-RNA or the YTH domain proteins separately. On the one hand, we observed no apparent binding between N-7 and FAM-m⁶A-RNA by directly titrating N-7 into a constant concentration of FAM-m⁶A-RNA *via* the FP binding assay (Fig. 4A). On the other hand, we investigated the interaction between N-7 and YTH domain proteins *via* the thermal shift assay.⁴⁸ As a positive control, we measured the thermal stabilization effect of the YTH^{YTHDF1} protein upon binding to m⁶A-RNA; incubation of 2 μM or 16 μM m⁶A-RNA significantly elevated the melting temperature of YTH^{YTHDF1} by 1.4 °C or 13.3 °C, respectively (Fig. S13, ESI†). Next, we characterized the effects of N-7 incubated with the five YTH domains. N-7 exhibited thermal stabilizations of all five YTH domain proteins; when 6 μM N-7 was incubated, the melting temperatures of the YTH domain proteins increased by 0.4–0.8 °C relative to the DMSO control (Fig. 4B and Fig. S14, ESI†). The stabilization effect became more prominent when an increasing amount of N-7 (50 μM) was added (Fig. 4B and Fig. S14, ESI†). In contrast, the negative control compound D-6 did not induce significant changes in the melting temperatures of the YTH domain proteins (Fig. S15, ESI†).

The thermal shift assay results suggested that N-7 inhibited the YTH and m⁶A RNA recognition likely through directly interacting with the YTH-domain proteins, rather than the RNA. The magnitude of melting temperature elevation caused by N-7 is significantly lower than that caused by the m⁶A-RNA binding; this is consistent with less favorable binding energetics between N-7 and the YTH domains compared to the

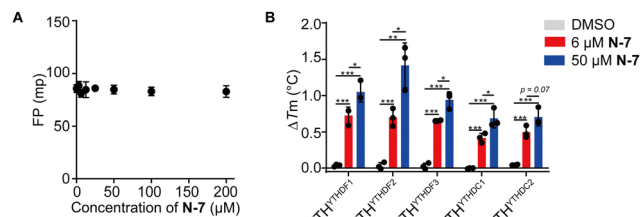


Fig. 4 N-7 directly interacts with YTH-domain proteins. (A) The FP binding data between N-7 and the FAM-m⁶A-RNA. Data are presented as mean ± SD with *n* = 3 biological replicates and no binding was observed. (B) The results of the thermal shift assay performed on YTH^{YTHDF1}, YTH^{YTHDF2}, YTH^{YTHDF3}, YTH^{YTHDC1}, or YTH^{YTHDC2} proteins in the presence of compound N-7 with varying concentrations. Data are presented as mean ± SD with *n* = 3 biological replicates. The two-tailed *t*-test was used to assess the statistical significance of the difference between two samples, with the *p*-value indicated as “ns” for *p* ≥ 0.05, “*” for *p* < 0.05, “**” for *p* < 0.01, or “***” for *p* < 0.001.

modified RNA. We reason that this change in energetics can result from weakened hydrogen bonding, van der Waals, charge–charge interactions, and/or a less favored hydrophobic effect for small molecule binding to the protein relative to the RNA.¹⁴

To gain further perspectives into potential structure–activity relationships (SAR), we performed an enrichment analysis of structure motifs in N-7, regarding the occurrence frequency of each motif in the overall library (320 compounds) *versus* that in the identified hits (13 compounds shown in Fig. S16, ESI†). Motif 1 (*i.e.* the purine) appears in 53% of compounds in the overall library and 100% of the screening hits with ~2-fold enrichment. This suggests that purine is an important fragment for the inhibitor structure, compared to pyrimidine-derived structures within the library. Despite the importance of purine, we found no inhibitory activity for the 6-methylamino purine (Fig. S16A, ESI†). This suggests the purine structure alone is not sufficient for presenting potency. Motif 2 (*i.e.* purine with the [1-(hydroxymethyl)cyclobutyl]methanol group) occurs in 10% of the overall library, of which the occurrence gets significantly enriched by >5-fold within the screening hits, where 54% (7 out of 13) of the hit compounds contain the Motif 2 structure. This suggests that Motif 2 can be critical for the binding with YTH domains. Only one compound (*i.e.* N-7) contains Motif 3 (*i.e.* purine with 2,7-diazaspiro[4,4]nonan-8-one) in the overall library (Fig. S16C, ESI†). It is difficult to assess any enrichment of this motif. Among the 13 hit structures, Motif 3-equivalent positions showed greater variability than Motif 2, suggesting a certain tolerance of chemical diversity for the substitutes at the C6 of the purine (Fig. S3A, ESI†).

Lastly, we conducted molecular docking of N-7 onto the reported high-resolution structure of the YTH domain of YTHDF1 protein (PDBID: 4RCJ) to speculate the potential binding mode.¹⁴ The best docking pose revealed that N-7 occupies the m⁶A binding pocket; the [1-(hydroxymethyl)cyclobutyl]methanol group of N-7 adopts the same orientation as the 6-methyl group of m⁶A (Fig. S17, ESI†). The docking result suggests potential polar contacts between two hydroxyl groups of N-7 with the backbone NH and C=O groups of C412, and the



side chain of D401 (Fig. S17, ESI†). The suggested binding pose indicates the critical role of Motif 2 for the compound binding to the YTH domain. Motif 3 orients outwards relative to the binding pocket, which is consistent with the chemical diversity we observed among the hit structures (Fig. S3A, ESI†).

The motif enrichment analysis of the screening results and molecular docking suggested Motif 2 can be a critical motif for binding to the YTH domain, whereas the spiro group of **N-7** can be more tolerating of diverse chemical groups. Future efforts in resolving the atomic-resolution structures of the **N-7**/YTH domain protein complexes and synthesizing **N-7** fragments and analogue compounds are critical for providing insights into the mechanism of inhibition and elucidating the structure–activity relationship.

Comparison of **N-7** with reported YTH domain inhibitors

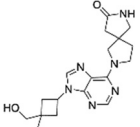
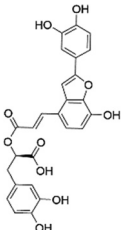
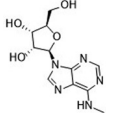
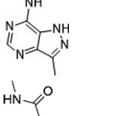
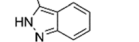
Next, we compared the inhibitory activity and selectivity of **N-7** with four reported YTH domain inhibitors that are commercially available, including the natural product “**SAC**”,³⁵ the “**m⁶A nucleoside**”,^{36,37} a pyrazolopyrimidine derivative compound “**6**”,³⁶ and an indazole derivative compound “**26**”.³⁸ These compounds were reported to inhibit YTH-m⁶A recognition against a single or subset of YTH domains in the literature, and the inhibitory activities (*i.e.* IC₅₀) were measured using different assays including AlphaScreen³⁵ and the homogeneous time-resolved fluorescence (HTRF) assay.^{36–38} As the IC₅₀ values

are difficult to compare when measured using different assay conditions, we systematically measured the inhibitory activities of four reported inhibitors with the same FP competition assay against five YTH domains (Table 1 and Fig. S18, ESI†).

Based on our FP competition assay results, **SAC** exhibited inhibitory activity with an IC₅₀ of 3.1 ± 2.5 μM against YTH^{YTHDF1}, consistent with the reported IC₅₀ value of 1.4 ± 0.2 μM within error measured by the AlphaScreen Assay (Table 1 and Fig. S18A, ESI†).³⁵ Our data suggest a weak selectivity of **SAC** against YTH^{YTHDF2}, which showed two times higher IC₅₀ compared to YTH^{YTHDF1}. Interestingly, we observed strong selectivity of **SAC** against YTH^{YTHDF3}, YTH^{YTHDC1}, and YTH^{YTHDC2} with IC₅₀ values ranging from 29 to 160 μM (Table 1 and Fig. S18A, ESI†). Unlike **N-7** being a *pan*-inhibitor, **SAC** presents selectivity among different YTH domains.³⁵ This immediately suggests different binding modes of **SAC** with YTH domains from those of **N-7**; high-resolution structural and biochemical characterizations would be critical to elaborate the differences in molecular recognition.

The **m⁶A nucleoside**, compound **6**, and compound **26** were identified and validated as binding fragments to YTH^{YTHDF2} and YTH^{YTHDC1} by high-throughput X-ray crystallography to aid structure-based inhibitor design for YTH domain proteins.^{36–38} These fragments show relatively weak inhibitory activities with the IC₅₀ values reported within the sub-millimolar to millimolar range as measured using the HTRF assay³⁸ (Table 1). Our

Table 1 Comparison of **N-7** with reported YTH inhibitors based on the FP competition assay. Data are presented as mean ± SD with *n* = 2 or 3 biological replicates

Compound name	Structure	IC ₅₀ (μM)				
		YTH ^{YTHDF1}	YTH ^{YTHDF2}	YTH ^{YTHDF3}	YTH ^{YTHDC1}	YTH ^{YTHDC2}
2-[9-[3,3-Bis(hydroxymethyl) cyclobutyl]purin-6-yl]-2,7-diazaspiro[4,4]nonan-8-one (N-7)		39 ± 3	34 ± 5	35 ± 5	48 ± 11	30 ± 7
(2 <i>R</i>)-3-(3,4-Dihydroxyphenyl)-2-[(<i>E</i>)-3-[2-(3,4-dihydroxyphenyl)-7-hydroxy-1-benzofuran-4-yl]prop-2-enoyl]oxypropanoic acid (SAC) ³⁵		3.1 ± 2.5 1.4 ± 0.2 ^a	6.0 ± 3.5 29.6 ± 3.7 ^a	106 ± 41	29 ± 4	160 ± 42
(2 <i>R</i> ,3 <i>S</i> ,4 <i>R</i> ,5 <i>R</i>)-2-(Hydroxymethyl)-5-[6-(methylamino)-9 <i>H</i> -purin-9-yl]oxolane-2,3-diol (m⁶A nucleoside) ^{36,37}		ND ^e	295 ± 84 504 ^b	ND	2342 ± 896 144 ^b	ND
<i>N</i> ,3-Dimethyl-2 <i>H</i> -pyrazolo[4,3- <i>d</i>]pyrimidin-7-amine (6) ³⁶		ND	ND	ND	2000 ± 1452 39 ^c	ND
<i>N</i> -Methyl-1 <i>H</i> -indazole-3-carboxamide (26) ³⁸		ND	ND	ND	3980 ± 1376 155 ^d	ND

^a Reported IC₅₀ value of **SAC** measured by the AlphaScreen assay in ref. 35. ^b Reported IC₅₀ value of **m⁶A nucleoside** measured by the HTRF assay in ref. 36 and 37. ^c Reported IC₅₀ value of compound **6** measured by the HTRF assay in ref. 36 and 37. ^d Reported IC₅₀ value of compound **26** measured by the HTRF assay in ref. 38. ^e ND, not detected by FP competition assay.



measurements showed very weak inhibitory activities of the **m⁶A nucleoside**, **6** and **26** against all five YTH domains ($IC_{50} > 2$ mM or not detectable), except that the **m⁶A nucleoside** shows an IC_{50} of 295 ± 84 μ M against YTH^{YTHDF2} (Fig. S18B, ESI†). Given the discrepancies in the IC_{50} values determined from the FP assay results and HTRF for compounds **6** and **26** against YTH^{YTHDC1}, we performed orthogonal competition REMSA to confirm the minimal inhibitory activity for compounds **6** and **26** (Fig. S19, ESI†). While these fragments (**6** and **26**) can fit into the binding pocket in the crystal structures,^{36,38} the molecules alone do not appear to have high inhibitory activities, which suggests additional interactions are required to compete with **m⁶A** RNA binding.

In summary, among the compared compounds, **SAC** and **N-7** are the most promising inhibitor structures. **SAC** contains more aromatic structures and presents a higher number of H-bond donors and acceptor groups than **N-7**, which can account for the selectivity among different YTH domains for **SAC** whereas **N-7** is shown to be a *pan*-inhibitor. The **N-7** structure may contain a robust motif that is important for binding to the highly similar pockets of all YTH domains.¹⁴ At the current stage, both **SAC** and **N-7** compounds showed *in vitro* inhibitory activities in the micromolar range and will benefit from further structure optimization efforts for improving potency.

Conclusions

This current work reports the discovery of a new nucleoside analogue structure **N-7** that functions as a *pan*-inhibitor for YTH domains recognition of **m⁶A**-RNA, with IC_{50} values in the range of 30–48 μ M. **N-7** exhibits a stabilizing effect of the YTH domains of human YTHDF1, YTHDF2, YTHDF3, YTHDC1, and YTHDC2 proteins as determined using a thermal shift assay, and no direct interaction was observed between **N-7** and RNA. This suggests that the inhibitory mechanism primarily arose from the affinities between the compound and the YTH domain proteins. We envision that the development of new small molecule inhibitors will largely facilitate research into uncovering precise functions of **m⁶A** modification in physiology and diseases, and potentiate future therapeutic efforts by targeting the epitranscriptome.

Experimental procedures

RNA oligonucleotides

RNA oligonucleotides including FAM-**m⁶A**-RNA, FAM-A-RNA, and **m⁶A**-RNA (Fig. 1C) were gifts from the He lab at the University of Chicago, which were originally produced in-house using an Expedite DNA synthesizer as previously reported.⁴⁹ We dissolved oligonucleotides into water (Fisher Science, BP561-1) for usage in *in vitro* assays.

Protein expression and purification

Genes of the YTH domain of YTHDF1 (amino acids 375–552), YTHDF2 (amino acids 383–553), YTHDF3 (amino acids 391–585), YTHDC1 (amino acids 345–509), and YTHDC2 (amino acids 1285–

1424) were cloned into a pET28a vector with an *N*-terminal His-tag for protein over-expression in *E. coli*, respectively (Fig. S1 and S5–S8, ESI†). We followed previously reported methods^{14,17,44} to over-express and purify the YTH domain proteins from *E. coli* BL21(DE3) cells. A 5 mL overnight cell culture was used for inoculating 1 L of LB medium with 30 μ g mL^{−1} kanamycin. The cells were cultured at 37 °C with shaking at 250 rpm until the OD₆₀₀ reached 0.6–0.8, which typically took around 3 hours. Subsequently, 0.5 mM Isopropyl β -D-1-thiogalactopyranoside (IPTG) was added into the cell culture to induce over-expression. Cells were then incubated in the shaker at 37 °C for 3 hours and then harvested by centrifugation at 2500 rpm for 20 minutes at 4 °C.

We prepared the lysis buffers for different YTH domain proteins based on the published protocols: 20 mM HEPES, pH 7.5, 200 mM NaCl, and 1 mM dithiothreitol (DTT) for YTH^{YTHDF1} and YTH^{YTHDF2} proteins⁵⁰ and 100 mM Tris-HCl, pH 8.0, 500 mM NaCl and 1 mM DTT for YTH^{YTHDF3} protein⁵¹ and 20 mM Tris-HCl, pH 7.5, 400 mM NaCl and 1 mM DTT for YTH^{YTHDC1} and YTH^{YTHDC2} proteins.^{44,52} The cell pellets were resuspended and lysed in the corresponding lysis buffer by sonication for each protein. Clear cell lysates were obtained by taking the supernatant after centrifugation at 11 000 rpm for 15 minutes at 4 °C. We then added 1% (w/v) streptomycin sulfate (Acros Organics) to the supernatant to precipitate genomic DNA, performed centrifugation at 11 000 rpm for 15 minutes at 4 °C, and recovered the supernatant afterward. The collected supernatant was subsequently incubated with pre-equilibrated His60 Ni Superflow Resin (Takara Bio) at 4 °C for 1 hour and then loaded onto an empty column; resins (bound with protein) were washed extensively using >20 mL of 10 mM imidazole solutions in the lysis buffer, and proteins were eluted under a gradient of imidazole concentrations (25 mM, 50 mM, 100 mM, 150 mM, 250 mM, and 500 mM) in the lysis buffer, and fractions of eluted proteins were collected into 2 mL tubes. All collected fractions were examined through 12% SDS-PAGE and those that contained predominantly the targeted protein were pooled together (Fig. S1 and S5–S8, ESI†), and concentrated using a concentrator (Sigma-Aldrich) down to around 3 mL. The concentrated protein was then desalted and exchanged into the storage buffer (25 mM HEPES, pH 7.5, 300 mM NaCl, 5% glycerol, 0.04% Triton X-100, and 1 mM DTT) using a PD-10 desalting column (GE Healthcare). The desalted proteins were concentrated to around 5 mg mL^{−1}, aliquoted, flash-frozen by liquid nitrogen, and stored at −80 °C. Protein concentrations were measured *via* absorbance at 280 nm with 1 absorbance unit approximated to 1 mg mL^{−1} protein using a Nanodrop spectrophotometer (Thermo Scientific).

The FTO protein was overexpressed and purified from *E. coli* BL21 (DE3) cells following previously reported methods.⁵³ Briefly, one liter of cell culture was grown at 37 °C for 3 hours in LB medium with 30 μ g mL^{−1} kanamycin until the OD₆₀₀ reached 0.6–0.8. Overexpression was induced by 0.5 mM IPTG and cells were incubated at 18 °C for 14–16 hours. Cells were lysed in 40 mL lysis buffer (20 mM Tris-HCl, 300 mM NaCl) by sonication, in the presence of a protease inhibitor and further purified with His60 Ni Superflow Resin. Proteins were eluted with 20 mM to 250 mM imidazole gradient in the context of the



lysis buffer followed by the desalting column and finally kept in a storage buffer composed of 50 mM Tris-HCl pH 7.5, 150 mM KCl, 5% glycerol, and 0.04% Triton-X-100 at -80 °C (Fig. S12, ESI[†]).

MS analysis of intact proteins

Purified proteins were analyzed using an Agilent 1260 Infinity HPLC coupled with the 6230 ESI time-of-flight (ESI-TOF) mass spectrometer (MS). The protein samples were subjected onto a C8 column (100 × 4.5 mm Phenomenex Aeris 3.6-μm Widepore XB-C8) and run through the column under an increasing gradient (5–95%) of non-polar buffer B in the aqueous buffer A (Buffer A: 95% water, 5% acetonitrile, 0.1% formic acid; Buffer B: 5% water, 95% acetonitrile, 0.1% formic acid). The eluted protein was injected into the MS and analyzed under the positive-ion mode. Total protein masses for the purified YTH domains and FTO were calculated through deconvolution using MagTran (Amgen).

FP binding assay for measuring binding affinities

Fluorescence polarization (FP) experiments were performed following the previously reported FP assay conditions for FAM-labeled RNA and YTH domains.^{50,54} Briefly, experiments were conducted in the binding buffer containing 25 mM Tris-HCl, pH 7.5, and 150 mM NaCl.⁵⁰ The same binding buffer was used in this study unless otherwise specified. RNA samples were diluted to 50 nM from the stock solutions by the binding buffer. YTH domain proteins were thawed, buffer exchanged into the binding buffer at 4 °C using the 10 kDa-cutoff concentrators (Sigma-Aldrich), and adjusted to 2× the highest concentration used in the binding assay. 1 μL RNase inhibitor (SUPERaseIn, Invitrogen) was added. 40 μL protein solutions with various concentrations were prepared by serial dilution using the binding buffer. Subsequently, we added 40 μL diluted RNA into each 40 μL protein solution, mixed, and incubated at room temperature for 30 minutes. The final concentration of FAM-m⁶A-RNA or FAM-A-RNA was constant at 25 nM, and the YTH-domain protein concentrations varied from 10 nM to 24 μM. We performed three biological replicates for each binding measurement using the same protein purified from different batches. After incubation, samples were transferred to a black polypropylene 384-well round-bottom plate (Cellvis) and FP was measured on a SynergyTM Neo2 Multimode Microplate Reader at the wavelength of 485/20 nm for excitation and 528/20 nm for emission at 25 °C.

We used the following equation to calculate the FP signal,⁴³

$$FP = \frac{I_{\parallel} - G \times I_{\perp}}{I_{\parallel} + G \times I_{\perp}}$$

where I_{\parallel} and I_{\perp} refer to the parallel or perpendicular polarized light intensity, respectively, and we used 0.75 for the G -factor (G) calibrated based on the instrument guidance for the plate reader. The measured FP values at varying protein concentrations (x) were then fitted to the quadratic equation below describing single-site specific binding using the Levenberg–Marquardt non-linear curve fitting algorithm implemented in

the Origin 2022 software:

$$FP = B + C \times \left(D + K_d + x - \sqrt{(D + K_d + x)^2 - 4Dx} \right)$$

where D is the constant concentrations of FAM-m⁶A-RNA or FAM-A-RNA ($D = 25$ nM), B and C relate to the FP for free RNA and bound RNA, and K_d is the dissociation constant.

Binding between FTO and FAM-m⁶A-RNA was performed as described above in the 50 mM borate binding buffer (pH 7.5).

To evaluate the binding affinity between FAM-m⁶A-RNA and N-7, we prepared eight N-7 compound solutions in the same binding buffer with 5% DMSO with 0 to 400 μM concentrations *via* serial dilution. 20 μL of 50 nM of FAM-m⁶A-RNA was added to 20 μL compound solution. The final concentration for the FAM-m⁶A-RNA was 25 nM and that for N-7 ranged between 0 to 200 μM. Samples were incubated and FP was measured and analyzed as described above.

FP competition assays for dose–response measurements and screening

To set up the FP competition assay, we first used the non-fluorescent “m⁶A-RNA” (Fig. 1C) as a positive control inhibitor. We incubated 40 nM to 25 μM m⁶A-RNA with 2 μM YTH^{YTHDF1} and 25 nM FAM-m⁶A-RNA in the binding buffer with added RNase inhibitor at room temperature for 30 minutes. Samples were transferred onto the 384-well plate and measured on the plate reader as described above. We obtained the dose–response curves by plotting the FP values against concentrations of inhibitors. The inhibitory curves and IC₅₀ values were obtained using the “dose–response inhibition” model in GraphPad Prism 6.0TM. The same assay condition was used for benchmarking the competition assay for other YTH domains (Fig. S9B, ESI[†]), except that 10 μM YTH^{YTHDC2} was used instead of 2 μM due to the weaker binding affinity (or increased K_d) for YTH^{YTHDC2} to m⁶A-RNA compared to other YTH domains (Fig. S9A, ESI[†]).

To assess the performance of the FP competition assay for screening, we performed the assay with positive and negative control inhibitors 20 times each, where we used 20 μM non-fluorescent m⁶A-RNA and blank binding buffer as the positive and negative control, respectively. We calculated the Z' factor using the following equation⁴³ based on the measured FP of the positive and negative controls,

$$Z' = 1 - \frac{3 \times (SD_{\text{pos}} + SD_{\text{neg}})}{|M_{\text{pos}} - M_{\text{neg}}|}$$

where SD and M represent the standard deviations and means of the 20 repeated measurements.

We purchased the Nucleoside Mimetics library from Enamine which contains 320 compounds dissolved in DMSO at 10 mM. All stock solutions of small molecules were prepared in 100% DMSO unless otherwise specified. To perform screening compounds, we first prepared RNA–protein solutions on the 384-well plate with 33.6 μL per well. We added 1.4 μL 1 mM compound into the RNA–protein solutions in each well, with the final concentrations of the YTH^{YTHDF1}, FAM-m⁶A-RNA, and



each compound at 2 μM , 25 nM, and 40 μM , respectively. Each compound was screened in technical duplicates (Fig. 2). Meanwhile, DMSO and the non-fluorescent m⁶A-RNA were used as the negative and positive controls for the inhibitory activity on the same plate. The plate was incubated at room temperature for 30 minutes and subjected to the plate reader for FP measurements.

To perform dose-response measurements, we ordered 40 mg of **N-7** (Z2760966931) from Enamine. We examined the quality of purchased **N-7** through LC-MS and ¹H NMR spectroscopy (Fig. S4, ESI†). The dose-response FP competition assay was set up similarly to that described for the non-fluorescent m⁶A-RNA. Instead of the m⁶A-RNA, 1.5–200 μM **N-7** were incubated with 2 μM YTH domain proteins and 25 nM FAM-m⁶A-RNA in the binding buffer.

As IC₅₀ values may be subjected to changes under varying assay conditions, we performed several control conditions for the FP competition assay. Specifically, we adjusted the concentrations of the YTH domain proteins from 2 μM to the concentration around the K_d for each protein binding m⁶A-RNA (Fig. 1D and Fig. S10A, ESI†). Secondly, we tested the reported FP competition protocol which first incubated the compound with YTH domains, followed by adding the FAM-m⁶A-RNA³⁵ (Fig. S10B, ESI†). Under these conditions, the measured IC₅₀ values showed no significant changes (Fig. S10C, ESI†).

Reported inhibitors, compound **6** and compound **26**, were ordered from Chemspace (CSMB00010870727 and CSSS00000159915). The m⁶A nucleoside was ordered from AmBeed. Salvianolic acid C was ordered from MedChemExpress (HY-N0319). 6-(methylamino)purine was purchased from Fisher Scientific. The inhibitory activities of these compounds were examined using the same dose-response FP competition assay as for **N-7**.

RNA electrophoretic mobility shift assay (REMSA)

Competitive REMSA was performed by incubating 20 nM YTH^{YTHDF1} or YTH^{YTHDC1} with various concentrations of **N-7** (1–200 μM) and 25 nM FAM-m⁶A-RNA in a buffer containing 10 mM HEPES, 50 mM KCl, 1 mM EDTA, 0.05% Triton-X-100, 5% glycerol and RNase inhibitor, in a final volume of 20 μL . The reaction mixture was incubated at room temperature for 20 minutes, and then loaded onto an 8% polyacrylamide gel containing 0.2% glycerol. Electrophoresis was performed in 0.5× TBE buffer at 90 V and 4 °C for 60 minutes. FAM-m⁶A-RNA was detected using the ChemiDocTM MP imaging system (BIO-RAD) with the fluorescence blotting module.

Thermal shift assay

Thermal shift assays were set up according to the reported assay conditions using the SYPRO orange dye, which exhibited enhanced fluorescence in a more hydrophobic environment typically during protein unfolding.⁴⁸ For the positive control, we incubated 2 μM or 16 μM m⁶A-RNA with 4 μM YTH^{YTHDF1} in the binding buffer with added RNase inhibitor and 5× SYPRO orange dye (Invitrogen) at room temperature for 15 minutes. After incubation, the thermal shift assay was performed in the

QuantStudioTM 3 Real-Time PCR System (Thermo Fisher). Each sample was heated from 25 °C to 75 °C ramping by 0.2 °C s^{−1}; meanwhile, fluorescence intensities were recorded every 0.3 °C with the excitation and emission wavelengths at 470 nm and 570 nm, respectively. Data were first normalized by setting the highest and lowest fluorescence intensities in each melting run to 100% and 0%, respectively. Data were then fitted to obtain the melting temperatures (T_m) using the Boltzmann Sigmoid equation⁴⁸ within GraphPad Prism 6.0TM. As the YTH^{YTHDF1} protein specifically bound with m⁶A-RNA with $K_d = 0.8 \pm 0.2 \mu\text{M}$ through the FP binding assay (Fig. 1D), we expected the presence of m⁶A-RNA would promote the thermal stability of the protein. As expected, we observed that the addition of m⁶A-RNA showed significant stabilization of the YTH^{YTHDF1} (Fig. S13, ESI†).

To assess whether **N-7** interacted with the YTH domain proteins, we used the thermal shift assay to examine if there were any stabilization effects of the YTH domains by adding **N-7**. We incubated 6 μM or 50 μM **N-7** with 4 μM YTH^{YTHDF1}, YTH^{YTHDF2}, YTH^{YTHDF3}, YTH^{YTHDC1}, or YTH^{YTHDC2} under the same conditions without the RNase inhibitor as above. As a negative control, we added an equal volume of DMSO rather than **N-7** into each protein. The thermal shift assay measurements and analyses were performed in the same manner as described for the positive control. For each YTH domain protein, three biological replicates were performed to quantify the errors of the assay. The thermal stabilizations of the YTH domain proteins were analyzed by the change in the T_m (ΔT_m) as the difference between the T_m measured on the protein with **N-7** or DMSO, and the T_m of protein-only control (Fig. 4B and Fig. S14, ESI†). The interactions between **D-6** and YTH domain proteins were assessed using the same method as for **N-7** (Fig. S15, ESI†).

Molecular docking with AutoDock

The crystal structure of the YTHDF1 in complex with GGM⁶ACU (PDBID: 4RCJ) was chosen for molecular docking modeling.¹⁴ The structure was prepared for docking by removing water molecules and the bound RNA oligonucleotide GGM⁶ACU. The structure of **N-7** was prepared for docking by generating conformers and optimizing geometry by AutoDock4.⁵⁵ During molecular docking, the binding pocket of YTHDF1 was defined as 10 Å around the m⁶A binding site. The **N-7** ligand was docked against the defined pocket of the YTH^{YTHDF1} protein *via* AutoDock. The resulting binding pose of **N-7** with the most favorable docking score was reported and analyzed.

Author contributions

H. Z. conceived the idea of the project and supervised the research. C.-H. W. performed all the experiments and data analysis with help from H. Z. H. Z. and C.-H. W. wrote the manuscript.

Data availability

The data supporting this article have been included as part of the ESI.†



Conflicts of interest

H. Z. and C.-H. W. have filed a provisional patent application for the inhibitors described in this manuscript.

Acknowledgements

We acknowledge the financial supports provided by the National Institute of General Medical Sciences and Boston College. We thank the Office of the Vice Provost for Research at Boston College for providing the microplate reader used for the research. We thank Dr Qing Dai, Zhongyu Zou, and the He Lab at the University of Chicago for sharing the RNA oligonucleotides and plasmids for the YTH proteins used in this study. We thank Dr Thusitha Jayasundera, Lingchao Kong, and Xinyi Lyu for their assistance in collecting the LC-MS and NMR data for compound N-7. We acknowledge Prof. Jianmin Gao, Prof. Jia Niu, Prof. Eranthie Weerapana, and group members from the Zhou group for insightful discussions and advice. This work was supported by Boston College (the lab startup fund to H. Z.) and the National Institute of General Medical Sciences (R35 GM150789 to H. Z.).

Notes and references

- 1 R. P. Perry and D. E. Kelley, *Cell*, 1974, **1**, 37–42.
- 2 R. Desrosiers, K. Friderici and F. Rottman, *Proc. Natl. Acad. Sci. U. S. A.*, 1974, **71**, 3971–3975.
- 3 D. Dominissini, S. Moshitch-Moshkovitz, S. Schwartz, M. Salmon-Divon, L. Ungar, S. Osenberg, K. Cesarkas, J. Jacob-Hirsch, N. Amariglio, M. Kupiec, R. Sorek and G. Rechavi, *Nature*, 2012, **485**, 201–206.
- 4 K. D. Meyer, Y. Saletore, P. Zumbo, O. Elemento, C. E. Mason and S. R. Jaffrey, *Cell*, 2012, **149**, 1635–1646.
- 5 N. Liu, Q. Dai, G. Zheng, C. He, M. Parisien and T. Pan, *Nature*, 2015, **518**, 560–564.
- 6 N. Liu, K. I. Zhou, M. Parisien, Q. Dai, L. Diatchenko and T. Pan, *Nucleic Acids Res.*, 2017, **45**, 6051–6063.
- 7 X. Wang, Z. Lu, A. Gomez, G. C. Hon, Y. Yue, D. Han, Y. Fu, M. Parisien, Q. Dai, G. Jia, B. Ren, T. Pan and C. He, *Nature*, 2014, **505**, 117–120.
- 8 I. A. Roundtree, G.-Z. Luo, Z. Zhang, X. Wang, T. Zhou, Y. Cui, J. Sha, X. Huang, L. Guerrero, P. Xie, E. He, B. Shen and C. He, *eLife*, 2017, **6**, e31311.
- 9 H. Shi, X. Wang, Z. Lu, B. S. Zhao, H. Ma, P. J. Hsu, C. Liu and C. He, *Cell Res.*, 2017, **27**, 315–328.
- 10 X. Wang, Boxuan S. Zhao, Ian A. Roundtree, Z. Lu, D. Han, H. Ma, X. Weng, K. Chen, H. Shi and C. He, *Cell*, 2015, **161**, 1388–1399.
- 11 K. D. Meyer, D. P. Patil, J. Zhou, A. Zinoviev, M. A. Skabkin, O. Elemento, T. V. Pestova, S. B. Qian and S. R. Jaffrey, *Cell*, 2015, **163**, 999–1010.
- 12 D. P. Patil, C.-K. Chen, B. F. Pickering, A. Chow, C. Jackson, M. Guttman and S. R. Jaffrey, *Nature*, 2016, **537**, 369–373.
- 13 J. Liu, X. Dou, C. Chen, C. Chen, C. Liu, M. M. Xu, S. Zhao, B. Shen, Y. Gao, D. Han and C. He, *Science*, 2020, **367**, 580–586.
- 14 C. Xu, K. Liu, H. Ahmed, P. Loppnau, M. Schapira and J. Min, *J. Biol. Chem.*, 2015, **290**, 24902–24913.
- 15 S. Zaccara, R. J. Ries and S. R. Jaffrey, *Nat. Rev. Mol. Cell Biol.*, 2019, **20**, 608–624.
- 16 M. N. Flamand, M. Tegowski and K. D. Meyer, *Annu. Rev. Biochem.*, 2023, **92**, 145–173.
- 17 T. Zhu, I. A. Roundtree, P. Wang, X. Wang, L. Wang, C. Sun, Y. Tian, J. Li, C. He and Y. Xu, *Cell Res.*, 2014, **24**, 1493–1496.
- 18 H. Du, Y. Zhao, J. He, Y. Zhang, H. Xi, M. Liu, J. Ma and L. Wu, *Nat. Commun.*, 2016, **7**, 12626.
- 19 O. H. Park, H. Ha, Y. Lee, S. H. Boo, D. H. Kwon, H. K. Song and Y. K. Kim, *Mol. Cell*, 2019, **74**, 494–507e498.
- 20 S. H. Boo, H. Ha, Y. Lee, M.-K. Shin, S. Lee and Y. K. Kim, *Cell Rep.*, 2022, **39**, 110861.
- 21 W. Xiao, S. Adhikari, U. Dahal, Y.-S. Chen, Y.-J. Hao, B.-F. Sun, H.-Y. Sun, A. Li, X.-L. Ping, W.-Y. Lai, X. Wang, H.-L. Ma, C.-M. Huang, Y. Yang, N. Huang, G.-B. Jiang, H.-L. Wang, Q. Zhou, X.-J. Wang, Y.-L. Zhao and Y.-G. Yang, *Mol. Cell*, 2016, **61**, 507–519.
- 22 Y. Gao, G. Pei, D. Li, R. Li, Y. Shao, Q. C. Zhang and P. Li, *Cell Res.*, 2019, **29**, 767–769.
- 23 R. J. Ries, S. Zaccara, P. Klein, A. Olarerin-George, S. Namkoong, B. F. Pickering, D. P. Patil, H. Kwak, J. H. Lee and S. R. Jaffrey, *Nature*, 2019, **571**, 424–428.
- 24 J. Wang, L. Wang, J. Diao, Y. G. Shi, Y. Shi, H. Ma and H. Shen, *Protein Cell*, 2020, **11**, 304–307.
- 25 X. Dai, T. Wang, G. Gonzalez and Y. Wang, *Anal. Chem.*, 2018, **90**, 6380–6384.
- 26 Q. Zheng, H. Gan, F. Yang, Y. Yao, F. Hao, L. Hong and L. Jin, *Cell Discovery*, 2020, **6**, 12.
- 27 C. B. Woodcock, J. R. Horton, J. Zhou, M. T. Bedford, R. M. Blumenthal, X. Zhang and X. Cheng, *Nucleic Acids Res.*, 2020, **48**, 10329–10341.
- 28 T. Lence, J. Akhtar, M. Bayer, K. Schmid, L. Spindler, C. H. Ho, N. Kreim, M. A. Andrade-Navarro, B. Poeck, M. Helm and J.-Y. Roignant, *Nature*, 2016, **540**, 242–247.
- 29 H. Shi, X. Zhang, Y.-L. Weng, Z. Lu, Y. Liu, Z. Lu, J. Li, P. Hao, Y. Zhang, F. Zhang, Y. Wu, J. Y. Delgado, Y. Su, M. J. Patel, X. Cao, B. Shen, X. Huang, G.-l Ming, X. Zhuang, H. Song, C. He and T. Zhou, *Nature*, 2018, **563**, 249–253.
- 30 J. Liu, B. T. Harada and C. He, *Trends Cell Biol.*, 2019, **29**, 487–499.
- 31 R. Shi, S. Ying, Y. Li, L. Zhu, X. Wang and H. Jin, *Cell Death Dis.*, 2021, **12**, 346.
- 32 N. S. Gokhale, A. B. R. McIntyre, M. J. McFadden, A. E. Roder, E. M. Kennedy, J. A. Gandara, S. E. Hopcraft, K. M. Quicke, C. Vazquez, J. Willer, O. R. Ilkayeva, B. A. Law, C. L. Holley, M. A. Garcia-Blanco, M. J. Evans, M. S. Suthar, S. S. Bradrick, C. E. Mason and S. M. Horner, *Cell Host Microbe*, 2016, **20**, 654–665.
- 33 W. Zhang, T. Wu, Y. Zhang, W. Kang, C. Du, Q. You, X. Chen and Z. Jiang, *Bioorg. Med. Chem.*, 2023, **90**, 117373.
- 34 J. Liao, Y. Wei, J. Liang, J. Wen, X. Chen, B. Zhang and L. Chu, *Cell Death Discovery*, 2022, **8**, 137.
- 35 Z. Zou, J. Wei, Y. Chen, Y. Kang, H. Shi, F. Yang, Z. Shi, S. Chen, Y. Zhou, C. Sepich-Poore, X. Zhuang, X. Zhou,



- H. Jiang, Z. Wen, P. Jin, C. Luo and C. He, *Mol. Cell*, 2023, **83**, 4304–4317.
- 36 Y. Li, R. K. Bedi, F. Nai, V. von Roten, A. Dolbois, F. Zálešák, R. Nachawati, D. Huang and A. Caflisch, *Eur. J. Med. Chem. Rep.*, 2022, **5**, 100057.
- 37 F. Nai, R. Nachawati, F. Zálešák, X. Wang, Y. Li and A. Caflisch, *ACS Med. Chem. Lett.*, 2022, **13**, 1500–1509.
- 38 R. K. Bedi, D. Huang, L. Wiedmer, Y. Li, A. Dolbois, J. A. Wojdyla, M. E. Sharpe, A. Caflisch and P. Sledz, *ACS Chem. Biol.*, 2020, **15**, 618–625.
- 39 M. Micaelli, A. Dalle Vedove, L. Cerofolini, J. Vigna, D. Sighel, S. Zaccara, I. Bonomo, G. Poulentzas, E. F. Rosatti, G. Cazzanelli, L. Alunno, R. Belli, D. Peroni, E. Dassi, S. Murakami, S. R. Jaffrey, M. Fragai, I. Mancini, G. Lolli, A. Quattrone and A. Provenzano, *ACS Pharmacol. Transl. Sci.*, 2022, **5**, 872–891.
- 40 Y.-G. Hong, Z. Yang, Y. Chen, T. Liu, Y. Zheng, C. Zhou, G.-C. Wu, Y. Chen, J. Xia, R. Wen, W. Liu, Y. Zhao, J. Chen, X. Gao and Z. Chen, *Cancer Res.*, 2023, **83**, 845–860.
- 41 L. Wang, X. Dou, S. Chen, X. Yu, X. Huang, L. Zhang, Y. Chen, J. Wang, K. Yang, J. Bugno, S. Pitroda, X. Ding, A. Piffko, W. Si, C. Chen, H. Jiang, B. Zhou, S. J. Chmura, C. Luo, H. L. Liang, C. He and R. R. Weichselbaum, *Cancer Cell*, 2023, **41**, 1294–1308.
- 42 S. Yang, H. Zhang, Y. Li, F. Wang, G. Lin, T. Niu, H. Li, Y. Yi, H. Zhou, R. Yang, R. Yao, P. Zhou, Y. Li, M. Wu, M.-X. Chen, H. Xu, J. You, Y. Liao, C. Yang, A. Zhao, C. Chen, L. Li and Y. Wei, Discovery of a selective YTHDC1 inhibitor that targets acute myeloid leukemia, *Research Square*, 2023, preprint, DOI: [10.21203/rs.3.rs-2644364/v1](https://doi.org/10.21203/rs.3.rs-2644364/v1).
- 43 N. J. Moerke, *Curr. Protoc. Chem. Biol.*, 2009, **1**, 1–15.
- 44 C. Xu, X. Wang, K. Liu, I. A. Roundtree, W. Tempel, Y. Li, Z. Lu, C. He and J. Min, *Nat. Chem. Biol.*, 2014, **10**, 927–929.
- 45 X. Dai, T. Wang, G. Gonzalez and Y. Wang, *Anal. Chem.*, 2018, **90**, 6380–6384.
- 46 G. Jia, Y. Fu, X. Zhao, Q. Dai, G. Zheng, Y. Yang, C. Yi, T. Lindahl, T. Pan, Y. G. Yang and C. He, *Nat. Chem. Biol.*, 2011, **7**, 885–887.
- 47 Y. Huang, R. Su, Y. Sheng, L. Dong, Z. Dong, H. Xu, T. Ni, Z. S. Zhang, T. Zhang, C. Li, L. Han, Z. Zhu, F. Lian, J. Wei, Q. Deng, Y. Wang, M. Wunderlich, Z. Gao, G. Pan, D. Zhong, H. Zhou, N. Zhang, J. Gan, H. Jiang, J. C. Mulloy, Z. Qian, J. Chen and C. G. Yang, *Cancer Cell*, 2019, **35**, 677–691e610.
- 48 F. H. Niesen, H. Berglund and M. Vedadi, *Nat. Protoc.*, 2007, **2**, 2212–2221.
- 49 L. Hu, S. Liu, Y. Peng, R. Ge, R. Su, C. Senevirathne, B. T. Harada, Q. Dai, J. Wei, L. Zhang, Z. Hao, L. Luo, H. Wang, Y. Wang, M. Luo, M. Chen, J. Chen and C. He, *Nat. Biotechnol.*, 2022, **40**, 1210–1219.
- 50 B. Liu, D. K. Merriman, S. H. Choi, M. A. Schumacher, R. Plangger, C. Kreutz, S. M. Horner, K. D. Meyer and H. M. Al-Hashimi, *Nat. Commun.*, 2018, **9**, 2761.
- 51 Y. Li, R. K. Bedi, E. V. Moroz-Omori and A. Caflisch, *J. Chem. Inf. Model.*, 2020, **60**, 5932–5935.
- 52 C. Ma, S. Liao and Z. Zhu, *Biochem. Biophys. Res. Commun.*, 2019, **518**, 678–684.
- 53 G. Jia, C. G. Yang, S. Yang, X. Jian, C. Yi, Z. Zhou and C. He, *FEBS Lett.*, 2008, **582**, 3313–3319.
- 54 H. Zhou, B. Sathyamoorthy, A. Stelling, Y. Xu, Y. Xue, Y. Z. Pigli, D. A. Case, P. A. Rice and H. M. Al-Hashimi, *Biochemistry*, 2019, **58**, 1963–1974.
- 55 G. M. Morris, R. Huey, W. Lindstrom, M. F. Sanner, R. K. Belew, D. S. Goodsell and A. J. Olson, *J. Comput. Chem.*, 2009, **30**, 2785–2791.

